Turk J Elec Eng & Comp Sci, Vol.18, No.2, 2010, © TÜBİTAK
doi:10.3906/elk-0908-156

The effect of heat on the metallurgical structure and B-H characteristic of (stator) armature with iron-silicon alloy in electric machines

Fevzi KENTLİ, Ümit Kemalettin TERZİ
[1] *Department of Electrical Education - Faculty of Technical Education, Marmara University*
34722, Kadıköy, İstanbul-TURKEY
e-mail: fkentli@marmara.edu.tr, terzi@marmara.edu.tr

Abstract

Coils in electric machines are varnished for insulation after winding. These varnished coils are formed in stiff construction in slots. Under heavy-duty operating conditions, all or part of some coils may be burnt or broken. Thermal method is one of several ways to remove the defective coils. In this method, current is passed through the defective coils by an autotransformer (variac) until all the varnish of the coils is burned. If all the coils are out of order, the varnish is burned by replacing the stator or armature in a burning room. Consequently, defective coils in the stator (armature) slots can be easily removed. In this study, the latter way has been preferred and varnish of the damaged coils has been burned in a flame burning room to investigate the effect of heat on both the metallurgical structure and the magnetic characteristics of stator (armature) iron core material after removal of the defective coils. The relation between the magnetic characteristics and the metallurgical structure of the material and their solutions have been examined under laboratory conditions.

Key Words: *Heat effect on material, magnetic (B-H) characteristic, microstructure of material, removal of the burned windings.*

1. Introduction

Electric motors and generators are varnished for insulation after winding. These varnished coils are formed in stiff construction in slot. Because of heavy-duty operating conditions, coils can break or burn out. There are several methods to remove defective coils, of which the termal method is but one. In the thermal method, either a voltage is applied to defective coils by using a high-power autotransformer (variac) and a short-circuit current is made to flow through the coil until all the varnish is burned off, or, if all of the coils are out of order, the varnish is burned by putting the stator or armature in burning room. After these processes, defective coils are easily removed.

In this study, the method of removing varnish in a flame burning room is studied and the effect of the heat applied in this stage to structure of material and magnetic characteristics of the armature have been investigated. The temperature applied to an iron-silicon alloy is about 350 - 400 °C for a duration of one hour. The relationship between the magnetic characteristics and metallurgical structure has been examined under laboratory conditions. It is seen that when heat of a tempurature around 350–400 °C is applied to Si-Fe alloy for one hour, the maximum magnetic flux density ($B_{\max}$) is decreased by approximately 3.6%. In other words, it is saturated more quickly. However, the value of residual induction (B_r) and coercive field (H_c) are higher when the coil is heated than when no heat applied.

Electric machines can be affected negatively by increased temperature, which is caused by both heavy-duty conditions and thermal operations, as investigated in this study.Another problem is thermal aging. The thermal aging process is always present and occurs even when the motor is not running, aging at the rate caused by the ambient temperature to which the winding and core is exposed to. When the motor is running, it operates under service factor conditions that are limited to a 155 °C (Class F) average temperature. Curves of temperature versus lifetime show that thermal aging increases logarithmically as temperature increases for all classes of motors (Class A- Class H). These curves assume that the life doubles for a 10 °C decrease in temperature.

Since lower operating temperatures normally translate into higher efficiencies and longer life [1], a basic understanding of the impact of motor temperature on the stator (armature) can help achieve improved motor life and performance.

2. Experimental studies

The experimental studies are concentrated on two basic subjects: one, investigating the effect of applied heat on the magnetic characteristics of the stator material, and two, investigating the effect of applied heat on the microstructure of the material.

2.1. Experimental studies on magnetic characteristics

To investigate the effect of applied heat on the magnetic characteristic of the stator material, hysteresis curves of stator material have been drawn using the Ballistic Ewing method both before and after heat application. To achieve this goal, primary and secondary windings were wound on unwound stator material of an induction motor. The windings were varnished and hysteresis curves were obtained. Then, heat of a temperature of 350 - 400 °C was applied to the stator for approximately one hour until all the varnish melted. (The melting process of the varnish was carried out in a burning room. During the burning process, in order to record the heat applied on stator material, temperatures at various parts of the stator material were measured by digital thermometers with thermocouples.) The burned windings were then removed from the stator. New primary and secondary windings with the same characteristics and qualifications as to that prior to applying heat were wound on the stator and new $B-H$ hysteresis curves were obtained.

The experimental setup using the Ballistic Ewing method is shown in Figure 1 [2]. It is not possible to measure B values directly using the Balistic Ewing Method. To obtain $B-H$ hysteresis curves and permeability (μ) versus H curves, first the magnetic field intensity (H) and magnetic flux density (B) values should be calculated. The equations used to calculate $B-H$ and the relation between γ and B are given below.

2.1.1. Determination of k_B and k_H coefficients used in calculation of B and H

As shown in Figure 1, if the total resistance of the recorder circuit is R_t , when B_1 and B_2 are induced in the secondary winding N_2 by the magnetizing currents I_1 and I_2 flowing through the primary winding N_1, respectively, q can be written as

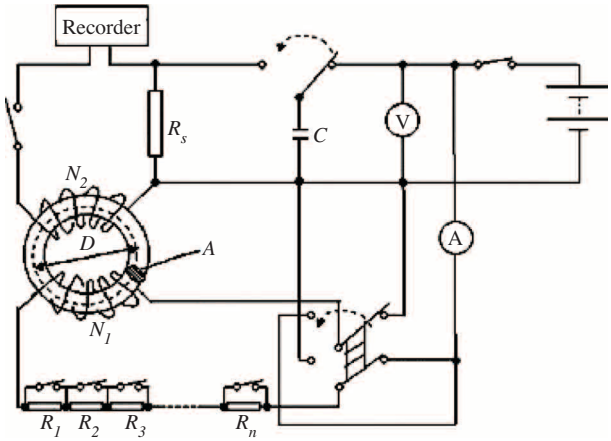

Figure 1. The experimental setup.

$$q = \int_1^2 i.dt = N_2.A.\Delta B/B_t \tag{1}$$

The deflection δ of the recorder (or ballistic galvanometer) in millimeters is

$$\delta = k_Q.q \tag{2}$$

The deflection δ_c for capacitor C [2] in millimeters is

$$\delta_c = k_Q.C.U.R_s/R_t \tag{3}$$

Thus,

$$\Delta B = (U.C.R_s/N_2.A.\delta_c).\delta = k_B.\delta \tag{4}$$

To make drawing easier, each B magnetic flux density can be described as;

$$B = k_B.\gamma \tag{5}$$

where γ is the virtual deflection drawn by the recorder in millimeters. Note that the value of γ is not the real deflection; the real deflections are δ deflections. The relation between δ and γ is given in Figure 2, where Σ δ and $B_{\max}$ are given in (6) as

$$B_{\max} = k_B.\gamma_{\max} = k_B.\Sigma \quad \delta \tag{6}$$

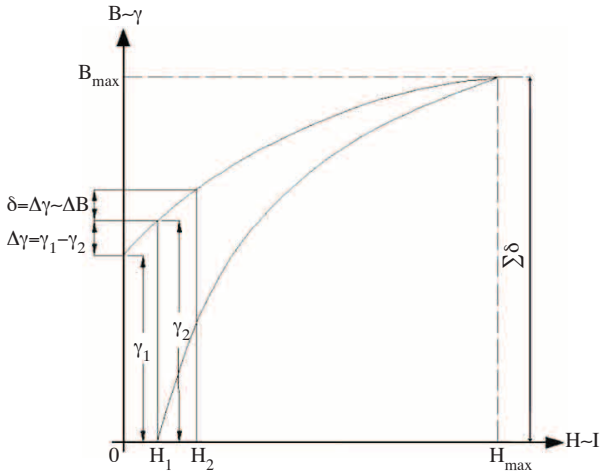

Figure 2. Relation between δ and γ.

For Figure 2, the following equations can be written:

$$\Sigma\delta = \delta_1+\delta_2+\delta_3+\cdots+\delta_{59}= \gamma_{max}= \gamma_{59} \tag{7}$$

$$\gamma_{58}= \gamma_{59}-\delta_{59}; \gamma_1= \delta_1; \gamma_2= \gamma_1+\delta_2 \tag{8}$$

The value of H that is used to draw the $(B-H)$ hysteresis curve can be calculated with the given formula in (9) as

$$H = N_1.I/\pi.D = k_H.I \tag{9}$$

where N_1=300 and N_2=234 are the number of turns on the primary and secondary windings; I is the current of primary winding; D =80.85x10^{-3} m is the average diameter of toroid (stator core); A =693.75x10^{-6} m^2 is the cross-sectional area of the toroid (stator core), neglecting any leakage fluxes that could be induced in the thooths; U =12V is the battery voltage applied to capacitor; C =1x10^{-6} F is the capacity of capacitor; R_s=100 Ω is the resistor connected in series to secondary winding; δ_c=0.16 mm is the deflection for the capacitor C (to make measurement of deflection easier, all of them have been enlarged by the same ratio); k_Q is the load constant of the recorder (or Ballistic galvanometer); k_B is the magnetic flux density coefficient; and k_H is the magnetic field intensity coefficient.

Thus, the coefficients k_B and k_H used in calculating B and H may be found using (4), (5) and (9) as

$$k_B= (U.C.R_s)/(N_2.A.\delta_c) = 0.0462 \text{ and } B = k_B.\gamma = 0.0462.\gamma \tag{10}$$

$$k_H = N_1/\pi.D = 1181.1127 and H = k_H.I = 1181.1127xI \tag{11}$$

2.1.2. Calculation of permeability μ

The average magnetic flux density (B_{av}) was used to calculate μ *as*

$$\mu = B_{av}/H = [B_{acc.} + (B_{dec.} - B_{acc.})/2]/H. \tag{12}$$

2.2. Experimental studies on metallurgical structure

To examine the effect of applied heat on the metallurgical structure of silicon-iron sheet metal and to determine the change in its chemical composition, chemical analysis and X-Ray difraction analysis of the material have been done before and after applying heat. Figure 3 shows the X-Ray difraction analysis showing the changes in its chemical composition. Also, Scanning Electron Microscope (SEM) micrographs from before and after heat application are shown in Figure 4.

For silicon-iron sheets before and after heat application, the results of chemical analysis are given in Table 1.

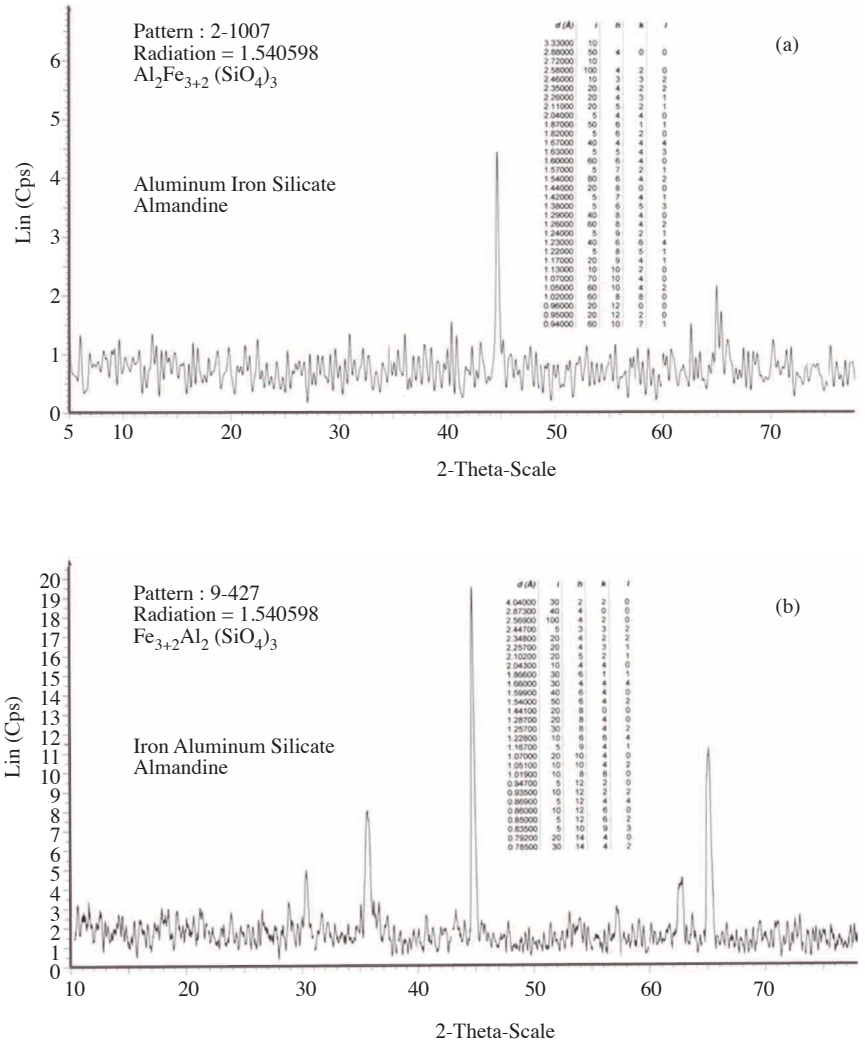

Figure 3. X-Ray diffraction analysis curves of (a) before and (b) after heat application.

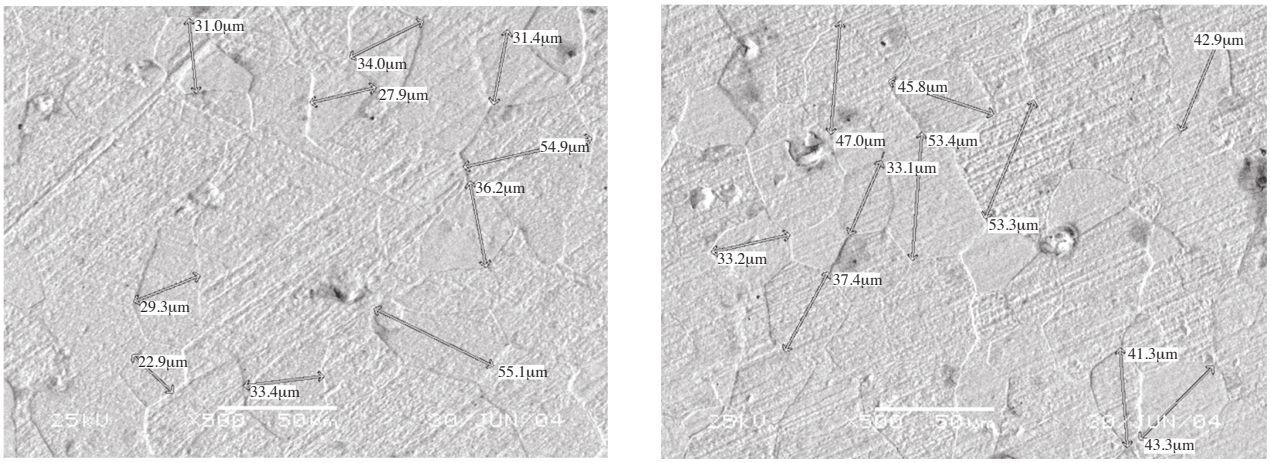

(a) (b)

Figure 4. Scanning Electron Microscope (SEM) micrographs of (a) before and (b) after heat application.

Table 1. The chemical composition of the silicon-iron sheet (a) before and (b) after heat application. (as average of 2 sparks) (as percentage of total weight)

	C	Si	Mn	P	S	Pb	Fe
a	0.002	1.78	0.214	0.00644	0.0149	0.002	97.61
b	0.002	1.71	0.217	0.00561	0.0128	0.002	97.68
	Cr	Mo	Ni	Al	Co	Sn	
a	0.0231	0.00623	0.0326	0.244	0.00476	0.003	
b	0.0242	0.00661	0.0321	0.243	0.00491	0.003	
	Cu	Nb	Ti	V	W	Sb	
a	0.0359	0.00214	0.001	0.001	0.005	0.00558	
b	0.0364	0.00204	0.001	0.001	0.005	0.0072	

3. Results and discussions

3.1. Results and discussion on magnetic characteristic

In electric generators and motors, one of the best techniques to find out the relationship between the electric circuit and magnetic circuit is to use hysteresis curves. A hysteresis curve is a method of evaluating the response of a material to the magnetic field. This response changes with temperature. Hysteresis properties of a ferromagnetic material are mostly determined by magnetic domain properties. Spontaneous magnetization depends on the temperature. After reaching its peak value at the absolute temperature, its value decreases with increasing temperature and becomes zero at the Curie point (also called the Curie temperature or critical temperature) [3].

Each magnetic material has a specific temperature, the Curie temperature, at which all magnetic properties are lost. The operating temperature of a magnetic material is well below this value. Thus, the Curie temperature is different for each material. For example, it is 770 °C (1418 °F) for iron and 740 °C (1364 °F) for Si-Fe alloy (unoriented and oriented) [4]-[7]. The Curie temperature is lowered by adding silicon. For a

10% addition of silicon to iron, the Curie temperature decreases from 770 °C to 600 °C [8]. In this study, the temperature applied to the silicon-iron alloy stator with 1.78% silicon is about 350-400 °C. Thus, because this value is below the Curie temperature, the stator does not lose its ferromagnetic properties.

The softest magnetic materials are iron-silicon alloys. Eddy-current and hysteresis losses are small in iron-silicon alloys. In this alloy, magnetic permeability is high. Iron- silicon alloys are used in sheet form. Rolling of the sheet is difficult because of the silicon content [9]. While increasing silicon levels results in increased alloy resistivity and decreased coercivity, the alloy ductility is significantly reduced with increasing silicon content. Therefore, while high resistivity and less coercivity is desired, the silicon level in the alloy cannot be increased beyond 3.5% if it is to be readily rolled into sheets [10]. Among various soft magnetic materials, electrical steels with 2.5-3.5% silicon are of great technological interest, particularly for electrical machine core applications, where they have enjoyed wide-spread popularity [11], [12]. In this study, an iron-silicon alloy, a soft magnetic material, with 1.78% silicon is used.

The differences between $B-H$ hysteresis curves measured before and after heat application show the effect of heat application during melting (burning) on the magnetic characteristics of the stator material. The difference between the two curves can be seen both on the size of the area bordered by the curves (that is, hysteresis loss) and on the location of the curves (the values of $B_{\max}$, H_c,-H_c). The area of the hysteresis loop is a measure of energy lost to heat per cycle of an alternating current. This is of great practical importance, since a magnetic material in an alternating field must dissipate this generated heat.

On some machines, it is essential to have some remanent magnetism to permit the self-excitation process to start. In a hysteresis loop, the energy represented by the area between the accelerating $B-H$ curve and the B axis is the energy supplied from source and the energy represented by the area between the decelerating $B-H$ curve and the B axis is the energy returned to source. Comparing the two areas reveals that the net energy consumption is equal to half the area of the hysteresis loop. Completing the cycle of magnetization will clearly require an energy represented by the whole loop. The whole area of the loop indicates the energy (power) loss in magnetic materials used for electrical apparatus.

Figure 5 and Figure 6 show the $(B-H)$ hysteresis curves, and Figure 7 shows the permeability versus magnetic field intensity curves. In this study, to see and compare the effect of heat application on hysteresis loss as a numerical value, two different methods were used. In the first method, the equations of accelerating and decelerating $B-H$ curves placed in first region both before and after heat application were obtained using a curve-fitting method. Then, the areas under the curves and the differences of these areas were evaluated by using these equations (i.e. by integrating). The second method is the trapezoidal method.

In the curve-fitting method, all curves are divided into six parts (a, b, c, d, e, f) to eliminate the match error, and the best curve-fitting equations were generated for each part. To provide exact matching, R^2 should be equal to 1 (where R^2 represents the regression). Then, the areas evaluated using these equations were summed. The best curve-fitting equations and their R^2 values, derived using the curve-fitting method for the first region, are given below. The absolute values of *-I (or B-H)* in third region are exactly the same, but they are negative.

H values for B_a are 259.842 A/m – 1074.8 A/m, for B_b are 1074.8 A/m – 2185.1 A/m, for B_c are 2185.1 A/m - 3720.5 A/m, for B_d are 3720.5 A/m – 5598.5 A/m, for B_e are 5598.5 A/m – 8102.4 A/m, for B_f are 8102.4 A/m – 10689 A/m. Thus, B values taken place in the group B_a are B_1 for 259.842 A/m, B_2

for 354.33 A/m, B_3 for 437.01 A/m, and B_{11} for 1074.8 A/m. B values taken place in the group B_b are B_{11} for 1074.8 A/m, B_{12} for 1169.3 A/m, B_{13} for 1263.8 A/m, and so on.

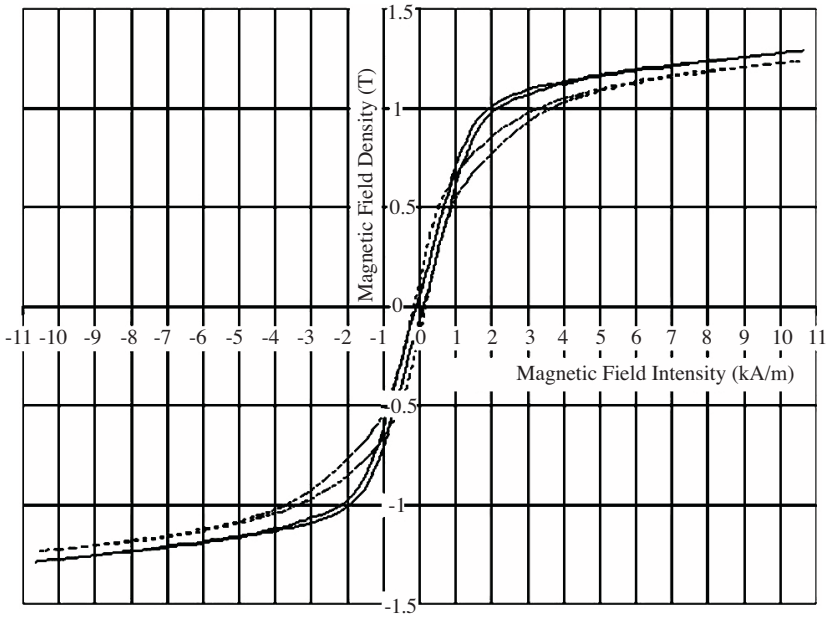

Figure 5. $(B-H)$ hysteresis curves drawn using the experimental data values. (—- = before heat application, . . . = after heat application).

B equations and R^2 values for the accelerating $B-H$ curve and before heat application are

$$B_a = 0.4003 lnH - 2.1846 (R^2 = 0.9657) \tag{13}$$

$$B_b = 0.4987 lnH - 2.8080 (R^2 = 0.9875) \tag{14}$$

$$B_c = 0.1956 lnH - 0.4987 (R^2 = 0.9987) \tag{15}$$

$$B_d = 0.1563 lnH - 0.1751 (R^2 = 0.9988) \tag{16}$$

$$B_e = 0.1728 lnH - 0.3190 (R^2 = 0.9992) \tag{17}$$

$$B_f = 0.1901 lnH - 0.4748 (R^2 = 0.9985) \tag{18}$$

B equations and R^2 values for the decelerating $B-H$ curve and before heat application are

$$B_a = 0.3889 lnH - 1.9986 (R^2 = 0.9768) \tag{19}$$

$$B_b = 0.4115 lnH - 2.1118 (R^2 = 0.9783) \tag{20}$$

$$B_c = 0.1733 lnH - 0.2994 (R^2 = 0.9920) \tag{21}$$

$$B_d = 0.1499 lnH - 0.1111 (R^2 = 0.9987) \tag{22}$$

$$B_e = 0.1537 lnH - 0.1453 (R^2 = 0.9999) \quad (23)$$

$$B_f = 0.1822 lnH - 0.4018 (R^2 = 0.9985) \quad (24)$$

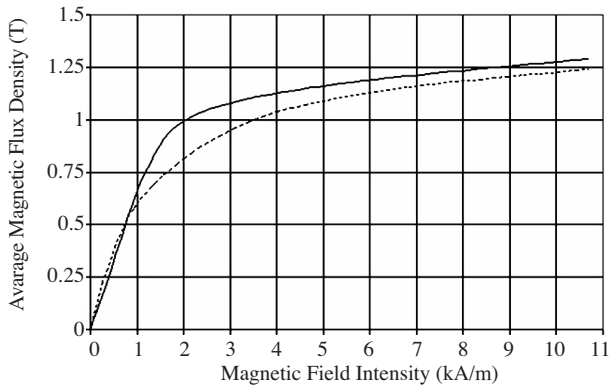

Figure 6. Average magnetic flux density versus magnetic field intensity curves drawn using the experimental data values. (—- = before heat application, ...= after heat application) (To calculate μ, the average value of B has been used).

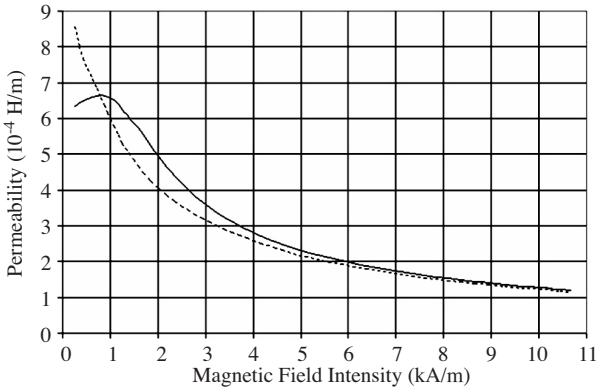

Figure 7. Permeability versus magnetic field intensity curves drawn using the experimental data values. (—- = before heat application, ...= after heat application)(To calculate μ,the average value of B has been used).

B equations and R^2 values for the accelerating $B-H$ curve and after heat application are

$$B_a = 0.3497 lnH - 1.8872 (R^2 = 0.9892) \quad (25)$$

$$B_b = 0.3391 lnH - 1.8052 (R^2 = 0.9998) \quad (26)$$

$$B_c = 0.3764 lnH - 2.0899 (R^2 = 0.9998) \quad (27)$$

$$B_d = 0.2550 lnH - 1.0890 (R^2 = 0.9957) \quad (28)$$

$$B_e = 0.2018 lnH - 0.6311 (R^2 = 0.9990) \quad (29)$$

$$B_f = 0.2001 lnH - 0.6185 (R^2 = 0.9985) \quad (30)$$

B equations and R^2 values for the decelerating $B-H$ curve and after heat application are

$$B_a = 0.2379 lnH - 0.9852 (R^2 = 0.9959) \quad (31)$$

$$B_b = 0.2828 lnH - 1.2963 (R^2 = 0.9992) \quad (32)$$

$$B_c = 0.2811 lnH - 1.2798 (R^2 = 0.9997) \quad (33)$$

$$B_d = 0.2153 lnH - 0.7399 (R^2 = 0.9996) \quad (34)$$

$$B_e = 0.1929 lnH - 0.5443 (R^2 = 0.9969) \quad (35)$$

$$B_f = 0.1834 lnH - 0.4619 (R^2 = 0.9985) \quad (36)$$

In the trapezoidal method, the curve between the measured γ deflection (or calculated magnetic flux density B) values was accepted as linear and so 59 trapezoids are formed for each B-H curve. Then, to calculate the area under B-H curve, the areas of all trapezoids were summed. Figure 8 shows a sample graphic illustrating the area calculation using the trapezoidal method.

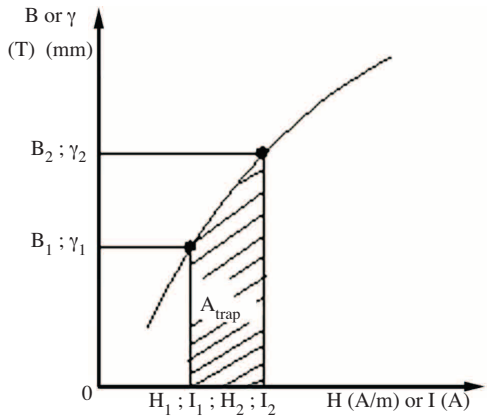

Figure 8. A sample graphic illustrating the area calculation according to the trapezoidal method.

The units of calculated area are not Watts in both methods. Moreoever, the units are not important because the ratio k is the parameter of interest. The value of k, calculated as $k = \mathrm{A}_a / \mathrm{A}_b$, where A_a is the area between two the $B-H$ curves after heat application, and A_b is the area between the two $B-H$ curves before heat application, is approximately the same for both methods and has a value of 1.77. At the same time, $k = \mathrm{P}_{h,a} \ / \ \mathrm{P}_{h,b}$, where $\mathrm{P}_{h,a}$ is the hysteresis loss after heat application, and $\mathrm{P}_{h,b}$ is the hysteresis loss before heat application. The value of k shows that the hysteresis loss with heat application is 1.77 times larger than without.

From the $B_{av} - H$ curves shown in Figure 6, while the variation of B_{av} with H from 0 A/m (or 0 T) to about 1000 A/m (or 0.65 T) is linear before heat application, it loses its linearity after heat application and from 0 A/m the variation is exponential.

The μ -H curves shown in Figure 7 are more interesting. The permeability of silicon-iron sheet metal before heat application starts at a value of 0.000615 H/m for a magnetic field intensity (H) of 260 A/m, and reaches its maximum value of 0.000665 H/m at about 790 A/m and returns to the same permeability value after heat application. It decreases regularly over the next H values and takes on a minimum value at 10,700 A/m and almost returns to the same level of permeability after heat application.

The shape of μ curve changes after heat application. The permeability has a maximum value for minimum H and a minimum value for maximum H, exhibiting an exponential variation. On the other hand, while the permeability of silicon–iron sheet metal at the H values between approximately 260 A/m and 750 A/m after heat application is gretater than before heat application, it decreases for values greater than 750 A/m and while H is increasing, the difference between two curves decreases.

The $B-H$ curve is divided into 3 main parts in theoretical analysis: 1) linear region, 2) knee (unstable) region, and 3) saturation region. Electric motors are designed to run in the linear region of the $B-H$ curve for operation stability and controllability. As shown in Figure 5, it is not possible to run in the linear region after heat application.

3.2. Results and discussion on metallurgical structure

Chemical analysis results did not indicate a high rate of change in composition at the elemental level. From a metallurgical point of view, at room temperature, silicon-iron sheet metals are in a body-centered-cubic crystal structured ferrite phase. Body-centered-cubic iron is one of the materials easily magnetized in the [100] direction.

The answer of the question "What is the relation between the ferromagnetic materials and magnetic field?" is important. Ferro-magnetic materials are spontaneously magnetized or self-saturating even in the absence of an external magnetic field, and these materials are divided into very small regions or magnetic domains, which are separated by domain walls. That is, magnetic domains are separated by the boundaries, known as domain boundaries or domain walls, whose thickness changes in the grain boundaries approximately in the range of 0.03 and 0.2 μm. Moreover, domains move opposite to each other in these boundaries. The schematic in Figure 9 illustrates the magnetic domains and the intervening boundary or domain wall.

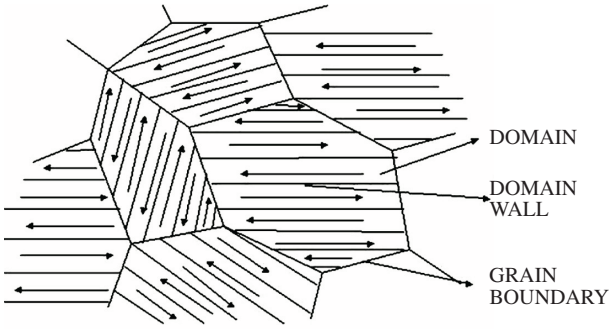

Figure 9. Magnetic domains inside a polycrystal-shematic.

Many magnetic domains can exist in a single grain. The direction of magnetization in a given domain is determined by the crystal structure of the material. Crystal anisotropy leads to magnetic anisotropy, thus certain crystal directions are easier to magnetize than others. In a given domain, the direction of saturation magnetization is one such easy direction of magnetization. For the specific case of an 180^0 wall, the direction of magnetization is exactly opposite for the two domains on either side of this interface. The direction of magnetization in the domain wall changes smoothly from one side to the other.

In the fully demagnetized state, each domain is magnetized to saturation by the internal molecular magnetic field, but the orientation of each magnetic domain is such that the net magnetization is zero. As a result of the strong molecular field there is complete alignment of all these molecular magnets in each domain. This gives the domain itself a definite magnetic axis, although the domains are lined up spontaneously. The reason for all this is that the overall system tends toward a minimum energy configuration. The application of an external field causes the various domain axes to line up with this field so that the resultant field becomes much more intense.

As the strength of the external applied field is increased, the remaining domains are forced to rotate such that their direction of magnetization is aligned with the applied field. Ultimately, when all the domains are lined up with the external applied field, the magnetic material is said to be saturated [13].

To explain the observed shape of the hysteresis curves, let us introduce the concept of magnetic domain rotation and wall motion. When the magnetic field is not applied, atomic dipoles occur at random directions. This situation causes thermal variation and is similar to material imperfection. If the magnetic field is poor, the dipoles partially get in order.

In general, domain wall motion is the predominant phenomenon observed up to the knee of the B vs. H curve for a poly-crystalline material. Above this point, magnetic domain rotation is needed to cause a small change in B (or more correctly M). The schematic in Figure 10 should be regarded as a guide only, since some degree of domain rotation or wall motion can occur above or below this line. It should be understood that no physical movement of atoms or change in crystal structure takes place. It is the direction of the internal magnetic field (at a more fundamental level, a consequence of the nature of the electron spins and orbits) that is being modified. Since the domains are being forced to magnetize along harder crystallographic directions, the material changes.

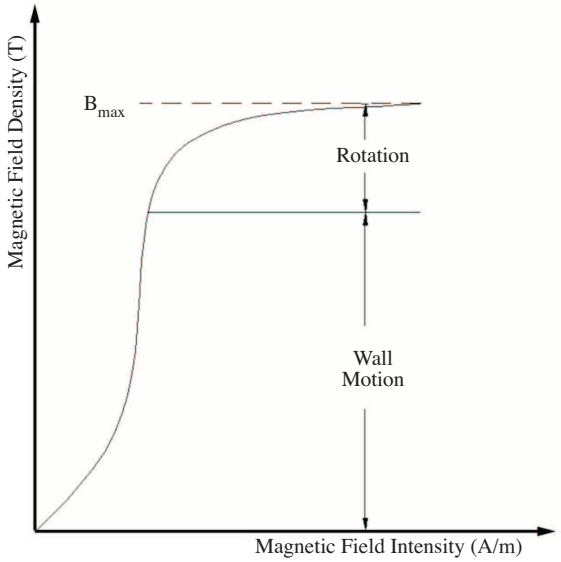

Figure 10. Shematic illustrating the regions of the hysteresis curve where domain wall motion predominates over domain rotation [14].

Above the knee of the hysteresis curve, the rotation of the miniature or elementary magnetic moments becomes increasingly more important. Eventually, the stronger external field aligns all the internal magnetic moments, and the material is said to be at saturation induction [13].

The heat applied to burn the varnished windings in this study was approximately 350-400 °C. This is not enough for phase transformation and no phase transformation was observed in microstructural examinating. This can be seen from Figure 3 showing X-Ray diffraction analysis.

The heat and the duration of heat application can be a driving force for diffusion. In this way, the grain size might change. The effect of grain boundary diffusion on grain size is important because it affects the domains in the grains and domain wall (boundaries). However, the variation of magnetization is very small at 400 °C. At 400 °C, the diffusion mechanism causes a decrease in vacancies and some ordering in dislocations. The diffusion mechanism also reduces atomic imperfections [15]. The small variation in grain size can be seen from Figure 4(b). The grain sizes increase after heat is applied.

4. Conclusion

The aim of this study is to investigate the effect of heat input applied to the stator of an electrical motor and generator during the removal process of defective windings, which can become defective under heavy-duty operating conditions, on the magnetic characteristic and metallurgical structure of a Si-Fe alloy. The effect of heat both on magnetic characteristic and on metallurgical structure are given in Figure 3-7 and Table 1, respectively. When Figure 3 and Figure 4 and Table 1 are examined, it is possible to gather that the chemical composition and microstructure of Si-Fe alloys do not change by heat. However, when examined in terms of magnetization, a slight change in magnetization is observed. Because the temperature is lower than the Curie Point, any changes (such as transforming to paramagnetic material) in the magnetic characteristic of material are not observed.

If Figure 5 is examined, it is possible to see that when the Si-Fe alloy is heated to around 350–400 °C for one hour, the maximum magnetic flux density ($B_{\max}$) is decreased by approximately 3.6%. In other words, it is saturated more quickly.

However, when heat is applied, the value of residual induction (B_r) and coercive field (H_c) are higher than when no heat is applied. That is, after heat application, the values of B_r and H_c increase 2.04 and 1.5 times, respectively, and increasing H_c is not a desired situation. Additionally, the area of the hysteresis loop (i.e. , hysteresis loss) when heat is applied is 1.77 times larger than when no heat is applied. Results also show that the hysteresis loss increases very slightly. At the same time, it can be stated that there is a very minor change in the Si-Fe alloy from soft magnet to hard magnet.

As can be seen from Figure 6, the $B-H$ curve loses its linearity in the previously linear region after heat application, following an exponential trend above 0 A/m. The motor was designed to run in the linear region of the magnetization curve, but this is not possible after thermal de-varnishing. Thus, the thermal de-varnishing is detrimental to motor performance.Moreover, the shape of the μ curve in Figure 7 changes after heat application, instead following an exponential trend.

Acknowledgment

The authors would like to thank Prof. Dr. Serdar Salman for his helpful comments on the manuscript.

References

[1] A.H.Bonnett. "Operating temperature considerations and performance characteristics for IEEE 841 motors." *IEEE Transactions on Industry Application*, Vol. 37, No.4, pp. 1120-1131, 2001.

[2] A. Dalfes. *Experiments of Electrical Measurement Laboratory, 4th edition.* Istanbul: Matbaa Teknisyenleri Basımevi, 1978.

[3] E. J. Thompson. *The Magnetic Properties of Materials.* London, 1967.

[4] H. N. Bertram, Z. Jin, V. L. Safonov. "Experimental and theoretical studies of thermal magnetization noise in GMR heads." *IEEE Transactions on Magnetics*, Vol. 38, pp. 38-44, 2002.

[5] G. Gogue. Motor design advancement using NdFeB magnets. Bebanon, Ohio: Motorsoft Company, 2000. Available: www. motiontraining.com/gogue/Lesson%201/page18.htm

[6] J. S. Barker. "Demonstrations of geophysical principles applicable to the properties and processes of the earth's interior." *Presented at the NE section GSA Meeting*, March, 1994. Available: www.geol.binghamton.edu/faculty/barker/demos/demo13.htm

[7] ——, *A critical comparison of ferrites with other magnetic materials*. Magnetics, Division of Spang & Company, Butler-PA, pp. 01-10, 2000. Available: www.mag-inc.com

[8] G. S. Avadhani. "Dynamic materials modeling technique for optimization of warm workability of armco iron and binary iron alloys." *Proc. Third International Conference on Mathematical Modeling and Computer Simulation of Materials Technologies (MMT-2004)*, Ariel, September, 2004.

[9] N. Tsuya, K. I. Arai, K. Ohmori, H. Shimanaka, T. Kan. "Ribbon-form silicon-iron alloy containing around 6% silicon." *IEEE Transactions on Magnetics*, Vol. Mag-16, No.5, pp. 728-733, 1980.

[10] Y. Birol, N. Parkan, O. Çakır. "Yüksek Silisli Elektrik Çeliklerinin Üretiminde Hızlı Katılaştırma Uygulaması." *Proceedings of the 9th International Metallurgy and Materials Congress*, İstanbul, Turkey, June 1997.

[11] K. Honma, T. Nozawa, H. Kobayashi, Y. Shimoyama, I. Tachino, K. Miyoshi. "Development of Non-Oriented and Grand-Oriented Silicon Steel." *IEEE Transactions on Magnetics*, Vol. 21, No.5, pp. 1903-1908, 1985.

[12] A. J. Moses. "Electrical Steels: Past, Present and Future Developments." *IEE Proceedings*, pp. 233-245, 1990.

[13] C. Lall. *Soft Magnetism Fundamentals for Powder Metallurgy and Metal Injection Molding*. New Jersey: Metal Powder Industries Federation, 1995.

[14] B. D. Cullity. *Introduction to Magnetic Materials*. Reading, MA: Addison-Wesley, 1972.

[15] A. Tekin, Material Science II, Istanbul Technical University, Istanbul, 1980.